Redundancy Control of a Free-Flying Telerobot

John R. Spofford
Martin Marietta Astronautics Group, Denver, Colorado 80201
and
David L. Akin
Massachusetts Institute of Technology, Cambridge, Massachusetts 02139

Manipulation from a free-flying vehicle has applications in space and undersea teleoperation. Both environments allow a vehicle to move freely in all six degrees of freedom. For many operations, such as inspection and servicing, the ability to manipulate from an undocked teleoperator will be essential. The major contribution of this research is the development of a control algorithm, *coordinated control*, which allows the simultaneous reduced-order control of a vehicle and attached manipulator. The entire telerobot system is controlled by commanding the end effector inertially with respect to the task. This is accomplished through a unified treatment of the vehicle and manipulator as a single dynamic system, based on considering the free-flying teleoperator as a redundant manipulator. The vehicle controller minimizes fuel expenditure while maintaining a desirable manipulator configuration. The coordinated trajectory algorithm is a blend of two modes: gradient pseudo-inverse trajectory control, which uses both vehicle thrust and manipulator motion, and reaction-compensation trajectory control, which allows the base to react freely to manipulator interaction torques. Blending between these modes occurs as a function of the teleoperator's configuration potential. The potential incorporates kinematic functions such as singularity avoidance, joint limits, and collision avoidance.

Introduction

THE space environment is inherently expensive to work in. The complexity and cost of maintaining humans in orbit preclude direct manual operations in some situations. Although it has often been demonstrated that human presence at a worksite is invaluable in emergencies, it is not always feasible to put humans there in the first place. As an example, high Earth orbits are unsuitable for sustained human presence due to radiation levels. Additionally the routine operational cost of a remotely operated robotic system in Earth orbit may be less than that of an astronaut. This is not to say that the performance of such a system is necessarily superior to a crewmember in a spacesuit, but that much more operational time may be available for the teleoperator.

The process whereby equipment performs maneuvering or manipulation tasks under the remote control of a human is

John Spofford is currently a research scientist with the Robotics group of the Martin Marietta Space Systems Company. He received S.B., S.M., and Sc.D. degrees in aeronautics and astronautics from the Massachusetts Institute of Technology in 1982, 1984, and 1988, respectively. He has been active in teleoperation research since 1981 in the MIT Space Systems Laboratory, where his work has included design and development of the Beam Assembly Teleoperator and a neutral buoyancy position and attitude sensor system. His current research interests include intelligent supervisory control, vehicle/manipulator control and dynamics, and space applications of teleoperation and robotics. He is a member of AIAA and IEEE.

David L. Akin is an assistant professor of aeronautics and astronautics at the Massachusetts Institute of Technology, where he is Associate Director of the Space Systems Laboratory. He received S.B., S.M., and Sc.D. degrees in aeronautics and astronautics from MIT in 1974, 1975, and 1981, respectively. His research spans the range of space operations from purely manual activities such as extravehicular activity, through teleoperation and robotics, to space applications of artificial intelligence techniques. He has also headed the development of the Beam Assembly Teleoperator and the Multimode Proximity Operations Device, two telerobot devices used in neutral buoyancy simulations of space operations. He was the principal investigator on the Experimental Assembly of Structures in Extravehicular Activity (EVA), a flight experiment onboard Space Shuttle mission 61-B. He is a member of the NASA Telerobotics Working Group and the NASA Advisory Council on the Role of Humans in Geostationary Orbit, and he has written over 30 papers on EVA, teleoperation, robotics, and space applications of artificial intelligence. Dr. Akin also is a member of AIAA.

Received Aug. 1, 1988; presented as Paper 88-4094 at the AIAA Guidance, Navigation, and Control Conference, Minneapolis, MN, Aug. 15-17, 1988; revision received Jan. 10, 1989.

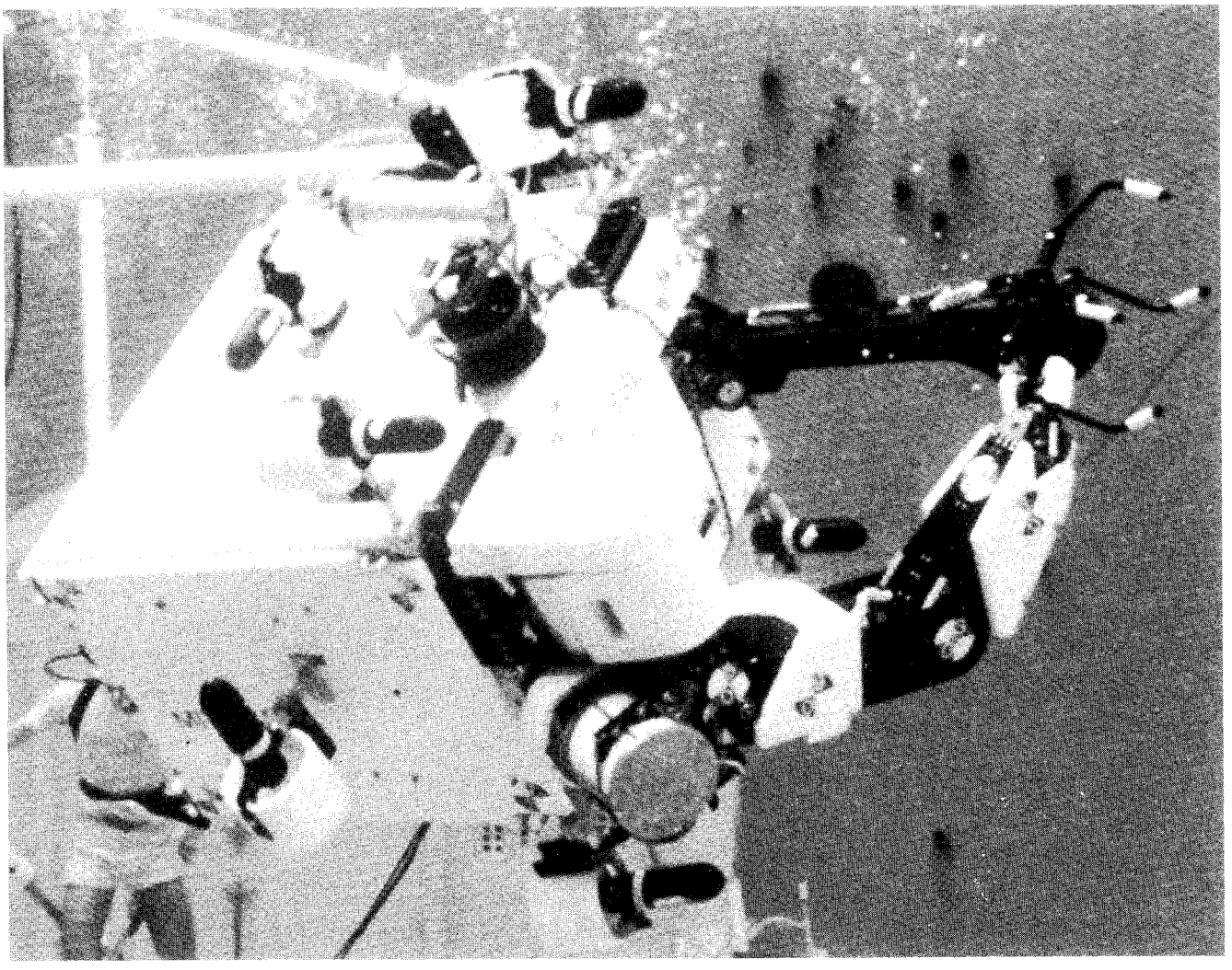

Fig. 1 Beam Assembly Teleoperator.

called teleoperation. Other terms currently in use include *telerobotics* (emphasizing autonomous capability of the equipment); *telemanipulation* (dexterous manipulation); and *telepresence* (realistic presentation of sensory information). This paper will use the term teleoperation to signify the combination of manipulation and maneuvering. A remotely controlled system capable of both maneuvering and manipulation is referred to as a teleoperator. Such a device is assumed to be commanded by a human operator rather than by an autonomous computer program.

Current plans for space teleoperators separate the operation of the system into two distinct phases: free-flying maneuvering and docked manipulation. It is the premise of this research that this constraint on the activity of the teleoperator unnecessarily limits its usefulness. There are many tasks, especially in contingency operations, where the ability to manipulate from an undocked teleoperator may prove essential. Examples of near-terms tasks suitable for teleoperation include inspection, surface treatment, and repair.[1]

Free-Flying Manipulation

Free-flying manipulation is applicable to teleoperation in space and underwater. Both environments allow a vehicle to move freely in all spatial degrees of freedom (DOF). Two significant advantages (or disadvantages) of the underwater environment are the presence of gravity and viscous drag. The separation of the vehicle's center of mass from its center of buoyancy creates a preferred orientation in two axes due to the action of gravity, which allows more effective attitude stabilization of the vehicle. Water drag is a significant factor in maneuvering, providing natural damping for vehicle translation (and rotation). These vehicles are generally designed to operate within a limited range of vehicle orientation, taking advantage of the natural attitude stabilization.

Teleoperators designed for space differ from their undersea counterparts in that the vehicle has no preferred orientation; all vehicle degrees of freedom must be actively controlled. The task of controlling a teleoperator is generally more difficult in space than underwater: in addition to the lack of a preferred orientation, there is no natural damping of vehicle motion. Space systems may be simulated on Earth underwater, in neutral buoyancy, for development and verification. Neutrally buoyant vehicles are balanced so that their weight matches their buoyancy, eliminating the effects of gravity. Additionally, the centers of mass and buoyancy must coincide to eliminate attitude preference. An example of such a telerobot system is the Beam Assembly Teleoperator (BAT), shown in Fig. 1 operating in the Neutral Buoyancy Simulator at the NASA Marshall Space Flight Center. This teleoperator was designed to perform structural assembly tasks in comparison with humans. The vehicle is a free-flying mobility unit with a full six DOF. BAT carries one dexterous manipulator and interchangeable specialized effectors. This system is described in detail elsewhere.[2] This work focuses on teleoperation in the 0-*g* drag-free space environment, but the results are generally applicable to undersea teleoperation as well.

With a vehicle/manipulator system, the human operator is presented with a formidable task: to try and manually control a system that might typically include 12 DOF or more. Typically this is done with separate controls for the vehicle and the manipulator. It is reasonable to expect that a control system that provides "task-relative" control, where only six DOF are necessary to specify effector motion relative to the task, would reduce the operator's work load. Independent continuous control of the vehicle and manipulator would require four, three-axis joysticks, occupying significant console space and requiring the operator to switch from one set to the other. One existing example of such a system is the Space Shuttle Orbiter; for satellite capture operations, the Shuttle is controlled from the starboard aft control station, whereas the remote manipulator system is controlled from the port aft station. This category of operation is thus a two-person task, with each person controlling two, three-axis hand controllers. It seems likely that this degree of crew involvement would be impractical for routine teleoperation tasks; crew productivity would improve if such a task were performed by a single person.

Six-axis displacement input devices are available for control input,[3] but currently available mechanisms occupy a significant volume in the control station. Two of these devices would be required, potentially causing workspace conflicts between the two. Six-axis force input devices require much less room but suffer from a modality mismatch between the force input and the displacement command. A control algorithm that allows an operator to command the entire teleoperator with the same control inputs required for either the vehicle or manipulator alone would be a significant advantage.

A free-flying teleoperator may be considered as a redundant manipulator, in that both systems have more controllable states than are necessary to specify the motion of the effector. One significant difference between the two is the use of reaction fuel for vehicle motion. In space this fuel must generally be launched into orbit, at a large cost, whereas electrical energy to operate the manipulator can be generated on-orbit. Any control system for a space teleoperator must consider the relatively large cost of vehicle motion.

Related Work

The development of computer-augmented supervisory control systems has been an active area of robotics research for several years. One application of such controllers has been to reduce the work load on the operator by assisting in the specification of manipulator motion from the task definition. During their review of man-machine interaction factors, Sheridan and Verplank[4] first noted the redundancy inherent in a free-flying teleoperator. The resolved-rate control algorithm, developed by Whitney,[5] was an early instance of a computer-aided control algorithm that allowed the operator to work in a task-referenced coordinate frame. Much work has also been done on redundant manipulation[6-8]—all directed at the case of extra manipulator joints.

The complications introduced by a free-floating manipulator base have been considered previously.[9-13] Longman et al.[10] developed compensated kinematics and reaction torques for a Shuttle-mounted manipulator. A kinematic controller that compensates for measured vehicle motion without utilizing the redundancy is presented. Knowledge of the mass and inertia properties of the manipulator and payload is assumed. The vehicle is assumed to be in an active attitude hold mode; the vehicle's DOF are not actively used. Recently, Vafa and Dubowsky[11] defined a virtual manipulator that combines the kinematic and dynamic properties of the manipulator and vehicle. This virtual manipulator's kinematic properties are a function of the real system's dynamic properties; the virtual base is inertially fixed at the system's mass center. This must be recalculated if the parameters of the physical system change (e.g., grasping or releasing a payload) and is restricted to noncontact situations. Yoerger and Slotine[12] have discussed supervisory control of redundant vehicle/manipulator systems for undersea tasks, based on a task-referenced potential field, but do not differentiate between vehicle and manipulator motion. Most recently, Alexander[13] has extended the operational-space control method to redundant systems and applied it to a planar system with five DOF. This work experimentally demonstrated the control method using endpoint sensing, however, the vehicle DOF were not actively controlled.

Despite these excellent research efforts, the topic of actively controlling the motion of both vehicle and manipulator for space applications, with or without fuel minimization, has not been previously addressed.

Teleoperator Modeling

The first step in the analysis of free-flying teleoperators is to determine the equations of motion. The *forward kinematics* describe the inertial position and orientation of the manipulator gripper, or effector, in terms of the manipulator and vehicle state variables. The *inverse kinematics* determine the state variables necessary to obtain a given effector position and attitude. The *forward dynamics* describe the motion of the system in response to applied forces and torques.

Extension is made by considering the vehicular DOF as extra manipulator "joints."[9] These joints have kinematic transformations, but only the terminal joint has mass properties. The advantage of this form is the simple extension of existing serial linkage analysis techniques. A disadvantage is the singularity associated with a three-parameter description of three-dimensional rotation. A four-parameter kinematic description of vehicle rotation (e.g., quaternions), does not result in an inveritable inertia matrix. Analyzing the vehicle motion using the same formulation as for the manipulator simplifies the task.

The kinematics and dynamics of a two-dimensional system are easier to visualize and present; therefore this paper models a planar teleoperator. The vehicle and manipulator have three DOF each, giving the teleoperator a total of six. Figure 2 defines the reference frames and geometric parameters associated with this teleoperator. The states of this system and the effector location are

$$x = \begin{bmatrix} x_B \\ y_B \\ \theta_B \\ \theta_1 \\ \theta_2 \\ \theta_3 \end{bmatrix} \qquad y = \begin{bmatrix} x_E \\ y_E \\ \alpha_E \end{bmatrix} \tag{1}$$

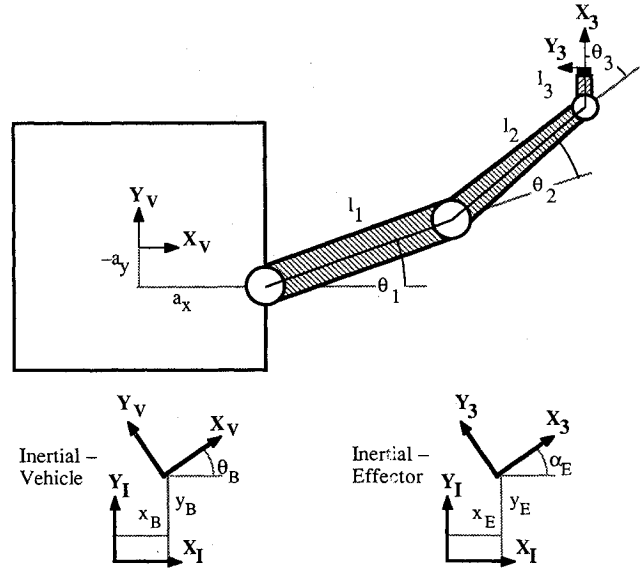

Fig. 2 Planar six-DOF coordinate frames.

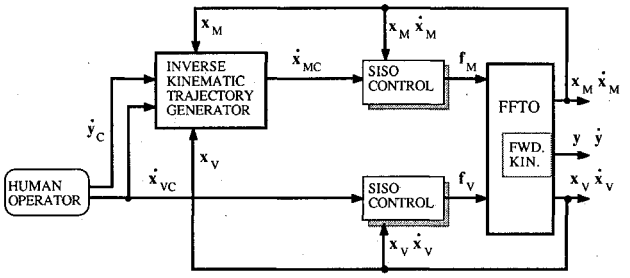

Fig. 3 Independent control block diagram.

This telerobot was simulated by a computer program, written in the C language, running on a Silicon Graphics IRIS workstation. Symbolic evaluation of the recursive dynamics formulation, using MACSYMA, reduced the real-time computations to a minimum. The full equations of motion are not presented due to space considerations; they may be found in Ref. 14. With the full nonlinear dynamics and a graphical display, the simulation ran at 7.5 Hz, fast enough for man-in-the-loop experiments.

Trajectory Control

This section is concerned with trajectory generation: the specification of a joint space trajectory to achieve the commanded effector trajectory. This involves a kinematic transformation from an inertial or effector trajectory with m components to a joint trajectory with n components. (In three dimensions, $m = 6$; in two dimensions, $m = 3$.) The spatial DOF m may be further divided into translational (m_t) and rotational (m_r) DOF. The n teleoperator DOF may be divided into vehicle (n_v) and manipulator (n_m) DOF. (Note that, for space systems, $n_v = m$, the spatial DOF. Available vehicle DOF for undersea systems may be limited if the vehicle's mass distribution is not rotationally neutral.) For all the teleoperators considered in this report, $n > m$. This makes the teleoperator redundant: the inverse kinematics are underdetermined. For a fully redundant teleoperator, with a full spatial set of arm DOF, $n = 2m$. A unique solution is thus possible only when additional constraints are imposed. The joint control problem is decoupled from the trajectory generation.

Independent Control Mode

Without supervisory control assistance, the vehicle and manipulator components of a teleoperator must be controlled separately. This will be referred to as the independent control mode. The vehicle will be directly controlled by the human operator, either in the vehicle reference frame or the inertial reference frame. The control of the vehicle is decoupled from the manipulator.

Figure 3 shows the structure of the independent control mode. The human operator provides one m-dimensional input vector to control the vehicle and another m-dimensional input vector to control the effector relative to the task. The controller determines the necessary manipulator commands to achieve the effector trajectory given the vehicle motion. In three dimensions, the operator must provide a total of 12 DOF; in two dimensions a total of six DOF are required. In this figure (and throughout the paper), boldface quantities are column arrays. The subscript V refers to vehicle states, M refers to manipulator states, and C denotes commanded values.

The inverse kinematic trajectory generator converts the order m effector command into an order n joint command; if the manipulator is redundant ($n_m > m$), then additional constraints must be applied by the controller. This is discussed later in the paper. The single-input/single-output (SISO) controllers drive the actuators. The nonlinear dynamics and kinematics of the teleoperator yield the actual system trajectory.

The control of the manipulator is kinematically much more difficult than that of the vehicle, which (in space) is basically an undamped second-order system responding to applied forces. Manipulator kinematics, as will be shown in subsequent sections on trajectory generation, are one source of these forces and torques.

Resolved-Rate Trajectory Generation

Initially proposed by Whitney,[5] resolved-rate control exhibits certain advantages for remote manipulation. This approach allows control of the end-effector with reference to arbitrary coordinate frames. The method transforms the desired effector rate, specified in inertial space, into corresponding joint rates. Effector motion may also be specified in the effector reference frame by reordering the equation; however, the independent control mode developed in this report defines effector motion in the inertial frame to match the operator's veiwpoint. Similarly, the vehicle trajectory may be specified in either the inertial or vehicle frames. The inertial frame is used herein to match the effector control.

When we work with a continuous kinematic formulation, the forward differential kinematics are

$$\dot{y} = J\dot{x} \tag{2}$$

The vector of end effector velocities $\dot{y}$ is of order m, and the vector of joint velocities $\dot{x}$ is of order n. (Here the generalized joint vector x includes both manipulator joints and vehicle DOF.) They are related by the differential forward kinematics matrix, the Jacobian J (of rank m). If the system is exactly determined, meaning that there is no redundancy and that the configuration is not singular, then the necessary joint velocities may be directly determined from the desired end effector motion

$$\dot{x} = J^{-1}\dot{y} \tag{3}$$

This method fails if the manipulator approaches a singular configuration. In this instance, the rank of J is no longer m.

The independent control mode is an enhancement of the resolved-rate strategy. Direct inverse position kinematics are used to compute the desired joint angles. The desired joint rates are computed via the Jacobian transform, using the current manipulator configuration. The command joint positions and rates are used by the joint controllers, as described later. It is convenient to separate the state vector and Jacobian into vehicle and manipulator components:

$$x = \begin{bmatrix} x_V \\ x_M \end{bmatrix} \qquad J = [J_V \quad J_M] \tag{4}$$

The block diagram of the inverse kinematic trajectory generator is depicted in Fig. 4. Note the independent solutions for the necessary joint positions and rates. This is possible when the manipulator is exactly determined: $n_m = m$.

$$\dot{y} = J_V\dot{x}_V + J_M\dot{x}_M \tag{5}$$

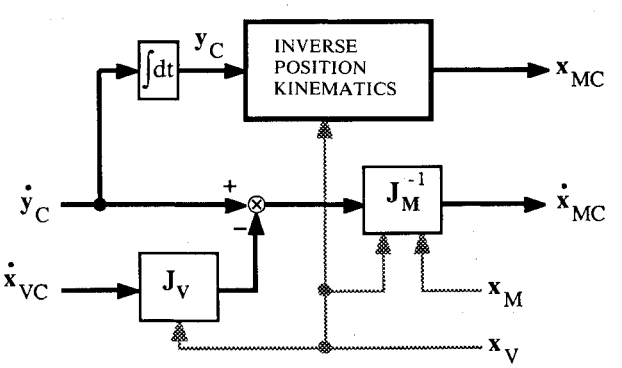

Fig. 4 Inverse kinematic trajectory generator.

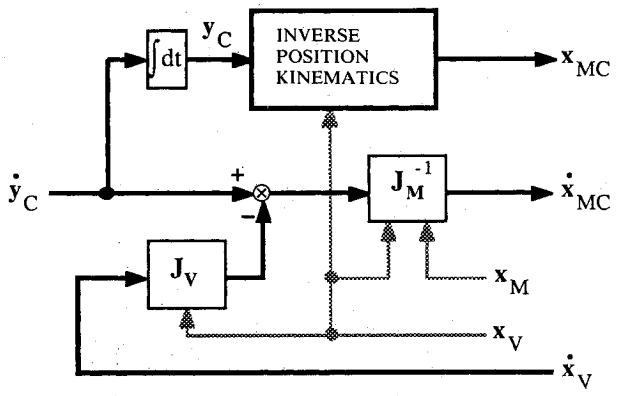

Fig. 5 Reaction-compensation trajectory generator.

This may be inverted for the manipulator joint rates, as long as the manipulator Jacobian is invertible (i.e., the manipulator is nonsingular):

$$\dot{x}_M = J_M^{-1}(\dot{y} - J_V \dot{x}_V) \tag{6}$$

This allows determination of the required manipulator motion ($\dot{x}_{MC}$) as a function of the command effector ($\dot{y}_C$) and vehicle ($\dot{x}_{VC}$) rates, and the current configuration $J(x)$:

$$\dot{x}_{MC} = J_M^{-1}(\dot{y}_C - J_V \dot{x}_{VC}) \tag{7}$$

The necessary joint positions are calculated using the appropriate manipulator-specific nonlinear equations. The base of the manipulator is determined using the measured vehicle position x_V.

Reaction Compensation Trajectory Generation

Reaction compensation is a special case of the independent control mode. As is the case with independent control, the effector is moved to the target point in inertial space. The difference is that reaction compensation does not use the vehicle's thrusters to maintain an arbitrary base position and orientation. Thus the vehicle moves in reaction to the effector forces and arm motion, and the manipulator trajectory planner must account for this motion to reach the inertial target point accurately. The advantage of this case is obvious: it uses no fuel. The disadvantage is that the effector workspace is limited and is smaller than if the vehicle were fixed. The dynamic effect that reduces the workspace is a function of the relative masses and inertias of the vehicle and manipulator and is configuration dependent. A suitable procedure for determining the effective workspace in reaction compensation mode has been described in Ref. 11. One significant drawback to this mode is its marginal stability. A free-flying teleoperator completely controlled by reaction compensation cannot recover if the center of mass is nonstationary.

Reaction compensation mode may be directly implemented by setting the vehicle actuator forces f_V to zero. The vehicle command position and velocity may be anything, as they have no effect. The effector command drives the manipulator but, without motion compensation, it will not reach the target. The preferred implementation is to set the desired vehicle rate to match the actual vehicle rate:

$$\dot{x}_{VC} = \dot{x}_V \tag{8}$$

This method allows this mode to be combined with another, as will be discussed later. The manipulator command is compensated for the *measured* vehicle motion:

$$\dot{x}_{MC} = J_M^{-1}(\dot{y}_C - J_V \dot{x}_V) \tag{9}$$

The system has n_m active DOF and n_v passive DOF with this control mode, which is depicted in Fig. 5.

Although not generally an effective control mode due to the limited workspace, reaction compensation mode does have applications. It serves as a check on the accuracy of computer simulations of the equations of motion because no external forces are applied. Thus the center of mass of the teleoperator should remain inertially fixed for all manipulator trajectories. This mode is also an essential component of the coordinated control mode, which is described in a subsequent section.

Pseudo-inverse Trajectory Generation

In this section the vehicle-manipulator combination is treated as a generalized redundant mechanism. The resulting "manipulator" has $n_v + n_m$ active DOF; joints are both vehicle axes and actual joints. As noted by Whitney,[5] redundant joint motion may be specified by adding a constraint that the joint velocities minimize a quadratic function. This was extended by Liégeois[6] to minimize a function of the joint angles.

Since the vehicle/manipulator system is redundant, the Jacobian cannot be inverted, as it is not square. The traditional approach is to define the pseudo-inverse of the Jacobian as

$$J^{\ddagger} = J^T(J\,J^T)^{-1} \tag{10}$$

and then to calculate the necessary joint motion from

$$\dot{x} = J^{\ddagger}\,\dot{y} \tag{11}$$

This serves to define the motion of all the joints and minimizes the quadratic function $\dot{x}^T\dot{x}$. Since the matrix $J^{\ddagger}$ is $n \times m$, but only has rank m, it has a null space of dimension $n - m$. Using a projection operator, an arbitrary vector ϕ (of dimension n) may be applied:

$$\dot{x}_C = J^{\ddagger}\,\dot{y}_C + (I - J^{\ddagger}\,J)\,\phi \tag{12}$$

This has the effect of modifying the commanded joint motion, without affecting the desired effector motion. The ϕ may be defined as

$$\phi = \beta\ \nabla_x V(x) \tag{13}$$

where β is a negative constant, ∇_x is the gradient with respect to x, and V is a smooth potential function of the generalized

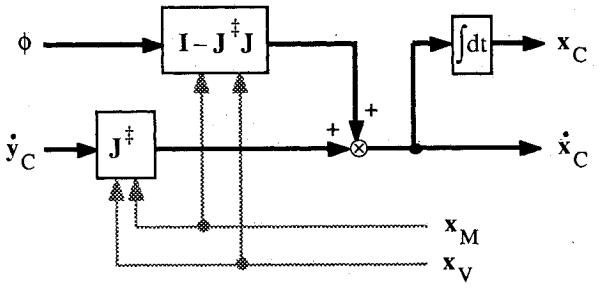

Fig. 6 Gradient pseudo-inverse trajectory generator.

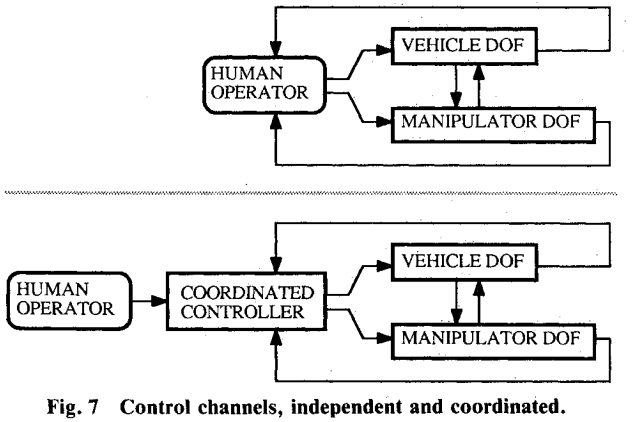

Fig. 7 Control channels, independent and coordinated.

joint variables. Individual terms of ϕ may be expressed as

$$\phi_i = \beta \frac{\partial V}{\partial x_i} \tag{14}$$

This definition of the null-space vector forces the joint motion $\dot{x}$ to reduce $V(x)$, without affecting $\dot{y}$. This feature of pseudo-inverse gradient control is an essential component of coordinated control, as will be discussed in the next section. A schematic of the controller is pictured in Fig. 6.

The disadvantage of this control algorithm, as applied to space teleoperators, is the excessive use of vehicle motion to achieve effector motion. One property of the inverse Jacobian approach is that the vehicle motion directly couples to effector motion. Thus when the Jacobian is inverted, whether redundant or not, the vehicle motion is the dominant factor. For tasks occurring inside the reach envelope of the manipulator, excessive vehicle motion wastes fuel. The advantage of the pseudo-inverse mode is the ability to command the effector to an arbitrary point with a single m-dimensional input vector. The coordinated control mode, which is presented in the next section, shares this advantage, but minimizes fuel use.

Coordinated Control

Without supervisory assistance, the operator must directly control all vehicle and manipulator axes. This would, in principle, require the control of $n_m + n_v$ DOF. It is more common, however, to resolve the manipulator and vehicle DOF into the m DOF workspace. In general, therefore, this requires manually controlling $2m$ DOF. With computer assistance, the operator need only control the m DOF relating the effector to the task; the coordinated controller handles the control of the rest of the system. Figure 7 illustrates the concept of reducing the number of channels controlled by the operator.

In this scenario the computer is acting as an assistant whose function is to keep the vehicle in a favorable position and attitude. The operator's control input device commands the end effector of the manipulator relative to the task. The vehicle is controlled by the computer supervisor without direct input from the human operator. This strategy is also applicable to hierarchical robotic control of a teleoperator. The specification of the effector trajectory may be separated from the configuration of vehicle and manipulator.

The primary task of the controller is to achieve the commanded effector position and attitude. Secondary tasks are to avoid joint limits, to maintain the vehicle within an allowed operating area, and to avoid the use of thrusters whenever possible. The approach taken in synthesizing a control system to satisfy these goals is to use a cost-function approach to do as much as possible on the secondary tasks while always performing the primary task.

Dynamic Blending: Coordination

It is desirable to combine the use of multiple actuators in a manner that avoids the use of actuators requiring propellant to produce force. A block diagram of the control structure developed to achieve these goals is shown in Fig. 8. This coordinated control mode, developed for the control of the manipulator-vehicle system, is based on two modes presented in the preceding section: reaction compensation and pseudo-inverse control. Reaction compensation mode (allowing the vehicle to freely respond to manipulator motions) uses no fuel at all, but results in a limited manipulator workspace. Pseudo-inverse mode (controlling both vehicle and manipulator in attitude and position) provides an infinite workspace but uses a lot of fuel. Both modes require measurement of the vehicle state, as does any closed-loop vehicle controller.

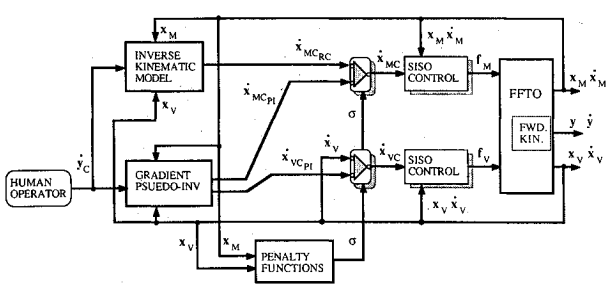

Fig. 8 Coordinated control block diagram.

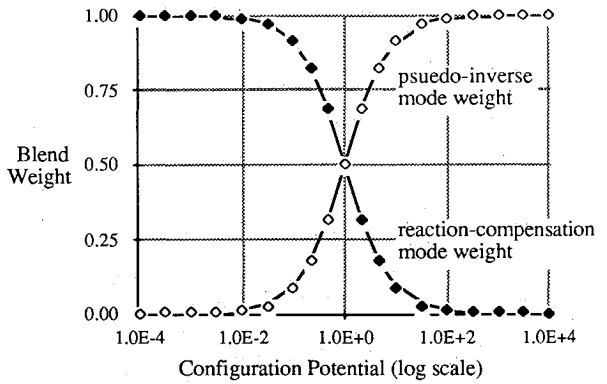

Fig. 9 Mode weights vs configuration potential.

The coordinated controller combines the contributions to the commanded state velocity from each submode, based on an overall potential function. Each subcontroller independently determines a desired state velocity which achieves the commanded effector motion. A suitable way to achieve the best of both modes is to transition smoothly between modes as an undesirable manipulator configuration approaches. This method, called "blending," is based on potential functions, which are presented in a subsequent section.

The blend method forms the commanded velocity based on the configuration potential σ. This potential is an arbitrary function of the system state and increases as the teleoperator approaches an undesirable configuration, such as manipulator singularity. The ability to define this potential function is an important feature of the coordinated control mode. At the same time, the selection of the proper potential function is essential to the successful functioning of this algorithm.

Coordinated control is based on a linear combination of control outputs of the two parallel systems to synthesize the control signal to the teleoperator. The rates commanded by the pseudo-inverse and reaction compensation controllers are $\dot{x}_{CPI}$ and $\dot{x}_{CRC}$, respectively. These are weighted by corresponding terms w_{RC} and w_{PI}. The synthesized command can be expressed as:

$$\dot{x}_C = w_{RC}\dot{x}_{CRC} + w_{PI}\dot{x}_{CPI} \tag{15}$$

Note that the two weights w_{RC} and w_{PI} must sum to one to achieve the commanded effector trajectory. When the weights are determined by blending, the terms are determined as follows:

$$w_{RC} = 1/(\sigma + 1) \tag{16a}$$

where $0 \leq \sigma < \infty$

$$w_{PI} = \sigma/(\sigma + 1) = 1 - w_{RC} \tag{16b}$$

When the potential is small, $\sigma \ll 1$, the command signal approaches the reaction compensation command. When the potential is large, $\sigma \gg 1$, the command signal approaches the pseudo-inverse command. Figure 9 plots the weights as a function of the configuration potential.

This combination of two commands to produce the applied command is possible because rates add linearly. This approach would not be feasible with the nonlinear equations relating

effector trajectories to state positions. Consequently, the SISO controllers integrate the command rate for the command position. The accuracy of this process is verified by comparing the inertial target position obtained by the forward kinematics to the position obtained by integrating the target rate.

System Potential Functions

The overall potential function is a kinematic function of the state variables with continuous first derivatives in all the variables. This function may consist of separate components related to specific kinematic functions. These may be defined based on the specific teleoperator design or as a function of the task. The potential function $V(x)$ developed for the planar system is constructed from three components:

$$V(x) = V_M + V_J + V_Z \tag{17}$$

referring to manipulator dexterity, joint positions, and vehicle position within an allowed zone. This group includes single and multiaxis functions in both joint space and the inertial reference frame. The only limitation in the choice of terms for the potential function is the requirement for continuous first derivatives. Each of these contributing potential terms is defined in the following subsections for the specific case of a planar telerobot.

In general, the function $V(x)$ is not a desirable quantity for the configuration potential: the minimum value is often nonzero due to conflicts between the various potential functions. A more useful form is the norm of the gradient of $V(x)$ with respect to x; this function is guaranteed to become zero for some system configuration. The gradient ϕ of the penalty function $V(x)$ is defined as

$$\phi = -\nabla_x V(x) = -\left[\frac{\partial V(x)}{\partial x}\right]^T \tag{18}$$

The transpose is necessary since the gradient ϕ is a column vector and the derivative of a scalar with respect to a column vector is a row vector. The configuration potential may then be defined as the norm of the gradient:

$$\sigma = \|\phi\| = \sqrt{\phi^T \cdot \phi} \tag{19}$$

which is zero at the minimum of $V(x)$.

Manipulability

The term "manipulability" has been defined as a quantitative measure of the dexterity of a manipulator.[15] This is defined to become zero at the edge of the workspace and to reach some maximum positive value inside the workspace. This has been previously applied to pseudo-inverse control as a means of defining the motion of redundant manipulators.[15,16] The manipulability w_m serves as an excellent penalty function for manipulator singularity:

$$w_m = \sqrt{\det(J_M J_M^T)} \tag{20}$$

where J_M is the manipulator Jacobian and is defined for manipulators with $n_m \geq m$. For computational efficiency, the square of this definition is used; this simplifies the derivation of the gradient

$$w = w_m^2 = |J_m J_M^T| \tag{21}$$

The manipulability potential function is defined to approach a large potential at the workspace edge. This is accomplished by inverting the squared manipulability w and multiplying by a gain k_M:

$$V_M = k_M/(w + \epsilon) \tag{22}$$

Numeric overflow is prevented by choosing a small positive value for the ϵ term. The gain k_M weights the effect of the manipulability potential relative to the other potential functions. The gradient of the potential is

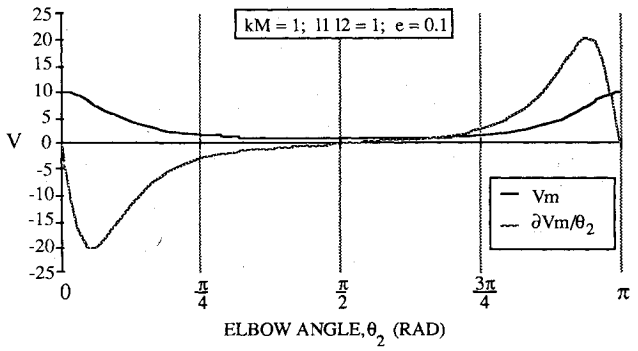

Fig. 10 Manipulability potential function.

$$\frac{\partial V_M}{\partial x} = \frac{-k_M}{(w+\epsilon)^2}\frac{\partial w}{\partial R}\frac{\partial R}{\partial J_M}\frac{\partial J_M}{\partial x} \tag{23}$$

where $R = J_M J_M^T$. The components of each term may be determined symbolically and then evaluated numerically for faster computation. The computation required can be reduced further by noting that R is symmetrical and has only $m(m+1)/2$ unique terms.

As an example, the manipulability is derived for the case of the planar teleoperator depicted in Fig. 2. The manipulator Jacobian is

$$J_M = \begin{bmatrix} -l_1 S_{B1} - l_2 S_{B12} - l_3 S_{B123} & -l_2 S_{B12} - l_3 S_{B123} & -l_3 S_{B123} \\ l_1 C_{B1} + l_2 C_{B12} + l_3 C_{B123} & l_2 C_{B12} + l_3 C_{B123} & l_3 C_{B123} \\ 1 & 1 & 1 \end{bmatrix} \tag{24}$$

where, for brevity, substitutions such as $s_{B12} = \sin(\theta_B + \theta_1 + \theta_2)$ are used. Applying Eq. (21), the manipulability simplifies to

$$w = (l_1\, l_2\, s_2)^2 \tag{25}$$

This means that the manipulator becomes singular when the first and second links align—when $\theta_2 = 0, \pm\pi$. The potential function and its derivative are plotted in Fig. 10. Since the potential is a function of only one state variable, there is only one component in the gradient for this case

$$\frac{\partial V_M}{\partial \theta_2} = \frac{-2k_M l_1^2 l_2^2 s_2 c_2}{[(l_1 l_2 s_2)^2 + \epsilon]^2} \tag{26}$$

The parameter ϵ controls the flatness of the gradient in the center of the range. When the norm of the gradient is used as the potential, there are stable equilibrium points at $\theta_2 = \pm\pi/2$ and unstable equilibrium points at $\theta_2 = 0, \pm\pi$. The joint will drive away from singularity as long as $\partial V_M/\partial\theta_2$ is negative for $0 < \theta_2 < \pi/2$; it is not necessary for the gradient to become infinite as $\theta_2 \to 0$.

Joint Limits

Manipulators have physical joint limits that prevent them from achieving arbitrary configurations. Incorporating a limit-related term into the cost function will force the controller to move other joints or the vehicle before the manipulator becomes "stuck." Another application is to restrict the vehicle rotational DOF within specified limits. A barrier func-

tion useful for quantifying proximity to the joint limits may be written as

$$V_J = \sum_{\text{joints}} k_{Ji} \vartheta_i^p \tag{27}$$

where

$$\vartheta_i = \frac{(x_{Hi} - x_{Li})^2}{4(x_i - x_{Li})(x_{Hi} - x_i)} \tag{28}$$

is the barrier function for each individual joint, p is a positive rational number, and x_{Hi}, x_{Li} are the upper and lower joint limits. An individual gain k_{Ji} may be specified for each joint. This is an "edge-based" potential. As the joint approaches a limit, the potential becomes infinite; in the center of the range, the potential is essentially flat. The gradient terms for the function are decoupled and are of the form

$$\frac{\partial V_J}{\partial x_i} = \frac{2pk_{Ji}(x_i - [(x_{Hi} + x_{Li})/2]}{(x_i - x_{Li})(x_{Hi} - x_i)} \vartheta_i \tag{29}$$

The gain k_{Ji} determines how close to the limit the controller will allow the joint to go before applying pseudo-inverse control. Note that the effects of the power p and gain k_{Ji} are combined. Figure 11 shows the pseudo-inverse mode weight as a function of pk_{Ji}.

Vehicle Position and Attitude

The vehicle is maintained in a permitted zone that specifies position, attitude, and a gradient. This zone is specified by the human operator analogically. This may be done using a hand controller or mouse and a graphics display; the control system maintains the specified center of the zone. This zone may be defined inertially or relative to the task, which may be moving. It is necessary to have sensory information about the position of the teleoperator vehicle for both cases; for the relative zone case information about the target is also required. The intent here is to allow the operator to define a zone of allowable vehicle motion that the controller will obey. This zone will be interactively defined by the operator with a graphics overlay on the task display. An advantageous method of generating a closed contour is to use cubic splines to connect control points. This method can be extended to three or more DOF, but three is the most that can be readily visualized. The vehicle rotational DOF may be decoupled from the translational, with either single-axis or coupled DOF limits. This potential function may be extended to treat the vehicle-zone interaction as a contour-contour problem, resulting in range from the nearest point on the vehicle to the contour, rather than as point-contour. The disadvantage of this is the computational complexity. This difficulty may be reduced by implementing the computation in hardware rather than software.

Results

The performance of the coordinated control mode was compared to the independent mode through simulations and manual control experiments. The performance was calculated based on time elapsed and fuel consumed. Detailed experimental procedures and results are presented in Ref. 14.

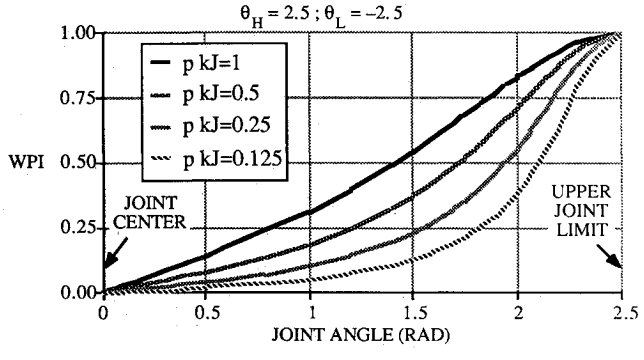

Fig. 11 Joint limit potential function.

Simulation

The best performance achievable with the coordinated control mode is not as good as the best possible independent mode performance. This is because the coordinated controller, with the same effector trajectory, does not recreate the optimal set of independent control inputs. Similarly, the best independent mode performance is not as good as can be achieved with open-loop control. The reason for this is the limited performance of the closed-loop controller. If a controller with infinite bandwidth and no actuator saturation were possible, the independent mode performance would approach the open-loop optimum.

For tasks in the usable workspace, the coordinated mode performance is superior to the independent mode in position/attitude hold and approaches the optimum independent mode. The performance advantage of the coordinated mode within the initial workspace increases with the trajectory velocity. For tasks beyond the initial workspace, the independent mode outperforms the coordinated mode with regard to fuel consumption. As the trajectory velocity of the large task decreases, the coordinated mode performance approaches that of the independent mode. The advantage of the coordinated mode is the smooth transition between modes with a spatial input; the independent mode requires more inputs to achieve the same range of motion.

Experimental

The experiment with human subjects indicated that the performance with the coordinated mode was only slightly worse than the independent mode. This was true for both tasks, although the difference between modes was not statistically significant. As an exception, the subjects with the worst overall score performed better with the coordinated mode at the more difficult task. Both tasks used the extended workspace of the teleoperator and required a roughly equivalent amount of vehicle motion in both coordinated and independent modes.

Based on the simulation results, it was expected that the subjects would perform significantly better with the independent mode than the coordinated mode. The experimental results indicated that the independent mode performance was only slightly better. This discrepancy indicates that the subjects generally were not able to take full advantage of the potential performance of the independent mode. The analysis strongly suggested that less experienced subjects performed better with the coordinated mode—especially at more difficult tasks. Thus, coordinated control will likely be advantageous in contingency operations where the operator has not been exhaustively trained beforehand.

As the complexity of the teleoperator system increases (e.g., from two dimensions to three dimensions), the advantage of coordinated mode's reduced-DOF inputs is expected to increase. Since the coordinated control mode only requires that the effector motion be specified relative to the task, the human operator's work load is independent of the number of teleoperator DOF. The ability to manipulate in an extended workspace, with only a single control input device, should prove invaluable.

Summary

The space environment introduces the possibility of performing manipulation tasks from a free-flying vehicle in addition to a more traditional docked configuration. Such free-flying manipulation capability raises new issues, such as vehicle fuel consumption and operator control work load. This paper has presented a new algorithm, referred to as coordinated control, for teleoperated control of such a vehicle and manip-

ulator system. This algorithm attempts to combine the best features of two alternative control modes which only require a spatial command set from the operator. Results to date indicate that the coordinated control algorithm improves the performance of the human-teleoperator system. It must be noted that this paper only presents results for a planar system. Verification and refinement for the three-dimensional case is necessary to determine real-world applicability.

Acknowledgment

The support of this work by the NASA Office of Aeronautics and Space Technology, under Grant NAGW-21, is gratefully acknowledged.

References

[1]Akin, D. L., Minsky, M. L., Thiel, E. D., and Kurtzman, C. R., "Space Applications of Automation, Robotics and Machine Intelligence Systems (ARAMIS)—Phase II," Space Systems Laboratory, Massachusetts Institute of Technology, Cambridge, MA, NASA CR-3734, 1983.

[2]Spofford, J. R., and Akin, D. L., "Results of the M.I.T. Beam Assembly Teleoperator and Integrated Control Station," AIAA Paper 84-1890, 1984.

[3]Brooks, T. L., and Bejczy, A. K., "Hand Controllers for Teleoperation: A State-of-the-Art Survey and Evaluation," Jet Propulsion Laboratory, Pasadena, CA, JPL Pub. 85-11, March 1985.

[4]Sheridan, T. B., and Verplank, W. L., "Human and Computer Control of Undersea Teleoperators," Man-Machine Systems Laboratory, Massachusetts Inst. of Technology, Cambridge, MA, ONR Contract N00014-77-C-0256, 1978.

[5]Whitney, D. E., "The Mathematics of Coordinated Control of Prosthetic Arms and Manipulators," *ASME Journal of Dynamics Systems, Measurement, and Control*, Dec. 1972, pp. 303-309.

[6]Liégeois, A., "Automatic Supervisory Control of the Configuration and Behavior of Multibody Mechanisms," *IEEE Transactions on Systems, Man, and Cybernetics*, Vol. SMC-7, 1977, pp. 868-871.

[7]Suh, K. C., and Hollerbach, J. M., "Local versus Global Torque Optimization of Redundant Manipulators," *Proceedings of the IEEE Conference on Robotics and Automation*, Inst. of Electrical and Electronics Engineers, New York, 1987, pp. 579-585.

[8]Yoshikawa, T., "Analysis and Control of Robot Manipulators with Redundancy," *Robotics Research: The First International Symposium*, edited by M. Brady and R. Paul, M.I.T. Press, Cambridge, MA, 1984, pp. 735-747.

[9]Spofford, J. R., *Dynamics and Control of Free-Flying Robots in Zero-Gravity*, S. M. Thesis, Department of Aeronautics and Astronautics, Massachusetts Inst. of Technology, Cambridge, MA, June 1984.

[10]Longman, R. W., Lindberg, R. E., and Zedd, M. F., "Satellite Mounted Robot Manipulators—New Kinematics and Reaction Moment Compensation," *International Journal of Robotics Research*, Vol. 6, No. 3, 1987, pp. 87-103.

[11]Vafa, Z., and Dubowsky, S., "On the Dynamics of Manipulators in Space Using the Virtual Manipulator Approach," *Proceedings of the IEEE Conference on Robotics and Automation*, Inst. of Electrical and Electronics Engineers, New York, 1987, pp. 579-585.

[12]Yoerger, D. R., and Slotine, J.-J. E., "Supervisory Control Architecture for Underwater Teleoperation," *Proceedings of the IEEE Conference on Robotics and Automation*, Inst. of Electrical and Electronics Engineers, New York, 1987, pp. 2068-2073.

[13]Alexander, H. L., *Experiments in Control of Satellite Manipulators*, Ph.D. Thesis, Department of Electrical Engineering, Stanford Univ., Stanford, CA, Dec. 1987.

[14]Spofford, J. R., *Coordinated Control of a Free-Flying Teleoperator*, Sc.D. Thesis, Department of Aeronautics and Astronautics, Massachusetts Inst. of Technology, Cambridge, MA, May 1988.

[15]Dubey, R., and Luh, J. Y. S., "Redundant Robot Control for Higher Flexibility," *Proceedings of the IEEE Conference on Robotics and Automation*, Inst. of Electrical and Electronics Engineers, New York, 1987, pp. 1066-1072.

[16]Klein, C. A., and Blaho, B. E., "Dexterity Measures for the Design and Control of Kinematically Redundant Manipulators," *International Journal of Robotics Research*, Vol. 6, No. 2, 1987, pp. 72-83.